AIChE

Experimental and Computational Study of the ''End of the Vortex'' Phenomenon in Reverse-Flow Centrifugal Separators

Gleb I. Pisarev, Vidar Gjerde, Boris V. Balakin, and Alex C. Hoffmann
Dept. of Physics and Technology, University of Bergen, Allegaten 55, 5007 Bergen, Norway

Henk A. Dijkstra
Dept. of Physics and Astronomy, University of Utrecht, Princetonplein 5, 3584 CC Utrecht, The Netherlands

Weiming Peng
Aker Offshore Partner AS, Sandslimarka 251, 5861 Bergen, Norway

Dept. of Physics and Technology, University of Bergen, Allegaten 55, 5007 Bergen, Norway

DOI 10.1002/aic.12695
Published online July 11, 2011 in Wiley Online Library (wileyonlinelibrary.com).

The ''end of the vortex'' (EoV) phenomenon, a flow instability that plays a crucial role in cyclone design and operation is studied in this article. In the experimental part of the study, tests were carried out to understand the origin and nature of the EoV and to study the effects of the flowrate through, and the length of, the cylindrical cyclone on the EoV. In the theoretical part, computational fluid dynamics (CFD) models, in agreement with the geometrical configurations and operating conditions used in the present and earlier experimental studies, were constructed and investigated. Three-dimensional simulations were carried out using the large eddy turbulence model with the commercial CFD package Star-CD. Bending of the vortex core to the wall of the vessel and its precessional motion, constituting the phenomenon of the EoV, was observed in the simulations in most geometries. The results are in a good agreement not only with the present experimental results but also with previous experimental observations. © 2011 American Institute of Chemical Engineers *AIChE J,* 58: 1371–1380, 2012
Keywords: cyclone, computational fluid dynamics, swirl tube, end of the vortex, vortex length, turbulence, large eddy simulation

Introduction

Reverse-flow centrifugal separators are widely used for dedusting and demisting gases in industry. There are many advantages over the other methods of separation.[1,2]

- They can operate under difficult conditions, for example, high temperatures and pressures or with chemically aggressive feeds.
- They have relatively low pressure drop.
- They are simple to construct.
- They are compact, which is important in many areas, for example, onboard ships.
- The collected material is unspoilt and suitable for return to the product stream, if relevant.

However, with all the advantages and the widespread applications there are some flow phenomena taking place in cyclones and swirl tubes that are crucial for their performance but difficult to understand and control. Perhaps the most important of these is the flow phenomenon known as the ''end of the vortex'' (EoV). This phenomenon occurs low in reverse-flow centrifugal separators such as cyclones or swirl tubes.

Correspondence concerning this article should be addressed to G. I. Pisarev at Gleb.Pisarev@ift.uib.no.

The EoV phenomenon takes place when, under some conditions, the vortex core deviates from the axis of the separator and attaches to the wall, where it rotates at some level above the bottom of the separator[3] (see Figure 1).

The distance from the bottom of the vortex finder (gas outlet) to the position of the EoV is often referred to as the ''natural vortex length,'' and the presence of the EoV influences several aspects of a cyclone's operation.[4]

- The separation space in the cyclone is assumed only to be effective above the EoV. This is normally taken into account in the modeling of cyclone performance simply by making the length of the cyclone equal to the natural length rather than the physical length of the separator.
- The transport of particles along the wall toward the dust exit is ineffective below the EoV; this may lead to clogging of the cyclone.
- The cyclone walls may be subject to severe wear at the position of the EoV. This becomes a problem if the separated particles are hard.

Most of the studies of the EoV have focused on the common cyclone with tangential inlet.[2,4–7]

We refer to a reverse-flow centrifugal separator as a ''swirl tube'' if the swirl is generated using swirl vanes rather than a tangential inlet and the body shape is cylindrical rather than cylinder-on-cone. The focus of this article is thus on a swirl-tube separator as the one sketched in Figure

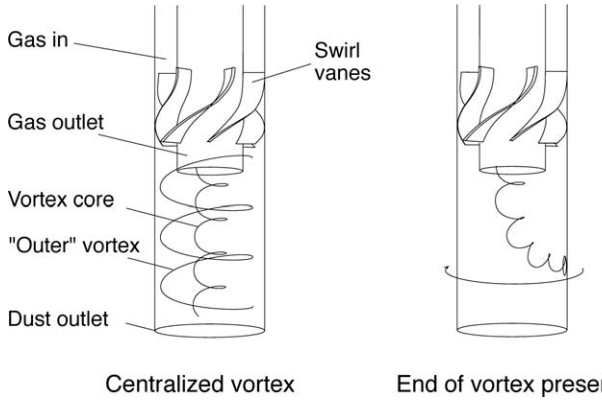

Figure 1. Illustration of the normal, centralized, flow in a reverse-flow swirl tube (left) and the flow when the EoV phenomenon is present (right).

1. Common to reverse-flow centrifugal separators is that from the inlet or swirl vanes the gas swirls downward in the outer part of the separator and the particles contained in gas are centrifuged to the wall. In the inner part of the separator, the gas reverses its axial flow direction and the cleaned gas exits through the central gas outlet as sketched in the left plate of Figure 1. The particles are transported along the walls and reach the bottom leaving through a special fitting or valve. The advantages of an axial inlet (swirl tube separator) is that it occupies less space than a tangential inlet. This is especially useful when operating in confined areas, for example, when having several separators working in parallel in a swirl deck. Also, better axial symmetry of the swirling flow is realized compared to tangential-inlet cyclones.

Experimental Setup

Figure 2 shows a sketch of the entire experimental swirl-tube setup. In this work, we were mainly interested in the gas flow pattern and specifically in the conditions at which the EoV phenomenon becomes apparent. Thus, the experiments were carried out with pure air without particles (except for trace amounts used for visualization in the bottom of the swirl tube, see below) and admixtures.

The experiments were carried out at ambient conditions. A centrifugal pump was located downstream of the separator and the air was thus drawn through the system by the lower pressure at the outlet. The flowrate was varied by adjusting two control valves as follows. Coarse changes to the flowrate were made using the main flow valve and for fine-tuning the bypass valve was used. The swirl tube was made of transparent plexiglas to allow visual observation of the flow field inside the separator. The roughness of the inner surface was estimated to be less than 1 μm. The shape of the separator was completely cylindrical. This simple design reduces the uncertainty caused by the geometry and is better suited for a fundamental study of the EoV phenomenon.

As can be seen in the figure, the gas flowed horizontally into the tube where the flow direction was changed to vertical, resulting perhaps in a less-than-optimal flow distribution to the vanes. This was mitigated by installing three vertical vanes above the swirl vanes to distribute the flow better over the annular cross-section.

One of the important parameters influencing the EoV is, as mentioned, the length of the separator. A range of swirl tube lengths were, therefore, studied. The length (from the bottom of the swirl vanes to the bottom of the tube) was varied from 35 to 95 cm in 10 cm steps. The diameter of the swirl tube used in this study was 10 cm. The other important design aspects for the swirl tube are the swirl vanes and the vortex finder. Figure 3 shows photos of the swirl vanes and the vortex finder used, along with sketches on which the dimensions are given.

The tangential component of the flow in the body of the swirl tube was brought about by swirl vanes at the inlet to the main body of the swirl tube. The vanes were mounted on the inner tube and swirl vane blades themselves were 1.25 cm wide. The vane pack represents the lowest cross-sectional area and the flow velocity is, therefore, higher in this region than everywhere else in the tube. The flow is assumed to quickly change from uniform, annular flow through the vanes to adopt a more Rankine-vortex-type of flow pattern below the vanes[8] and the vortex finder. The most important geometrical characteristic of the swirl vanes is the exit angle, which was 30° to the horizontal in our swirl tube.

The diameter and shape of the vortex finder plays a role in determining the vortex length[2,4,5,7] and is the most important factor in determining the separation efficiency and pressure drop in a given cyclone or swirl tube.[1,9,10] In this study, the vortex finder had a conical shape below the swirl vanes, finishing with cyclindrical section at its lower lip. This allowed us to investigate the EoV for a moderately narrow vortex finder with a relative diameter, D_x/D, of 0.4, where D is the diameter of the separator (see Figure 3).

The EoV also depends on the flowrate, which has to be measured quite precisely. In our experiments, this was done using a digital venturi meter.

Two ways of detecting the position of the EoV were used. To visualize the core of the vortex when it was at the bottom of swirl tube, that is, centralized, we added a very small amount (about 10 mg) of dust particles with diameter about 1 μm. It was assumed that this would not affect the flow pattern. For detecting the EoV on the wall of the swirl tube, pressure tappings were used. Small holes, 0.5 mm wide, were drilled every 3 cm along the separator body. These pressure tappings were connected to pressure transducers. The air velocity in the core of the vortex is very high and the static pressure is very low there. As the vortex core spins at a given axial position on the swirl tube wall, continuous pressure measurements at this position will detect the core as an intermittent pressure trough.[3] A burst of periodic

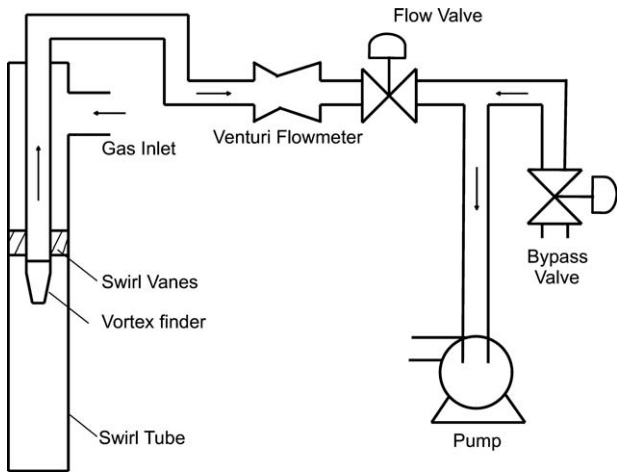

Figure 2. Schematic representation of the experimental rig.

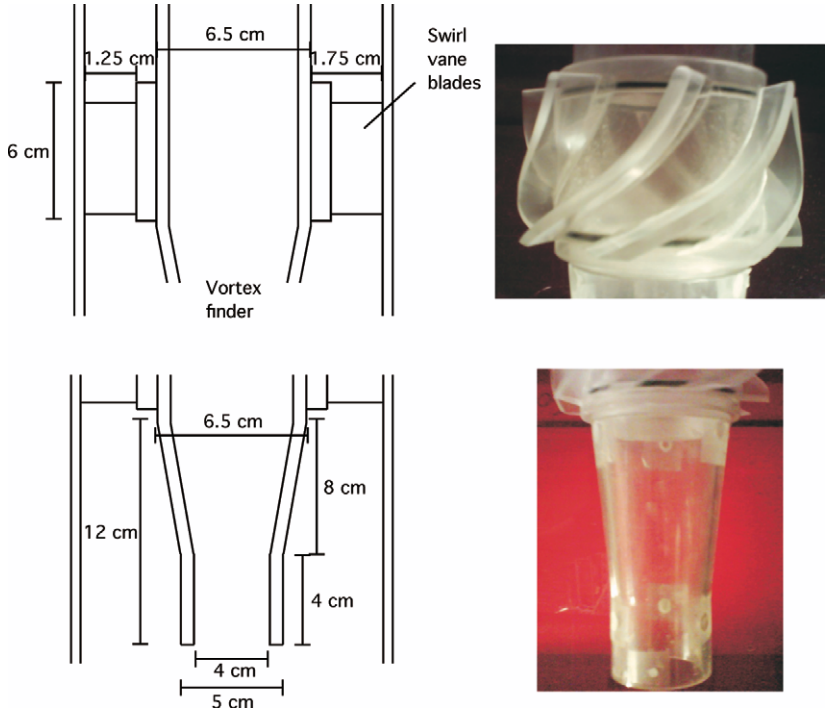

Figure 3. The swirl vanes (top) and vortex finder (bottom) used in this work.

[Color figure can be viewed in the online issue, which is available at wileyonlinelibrary.com.]

troughs in the pressure measured with high-speed pressure transducers at a given position thus indicates that the vortex core is passing this position and if the pattern continues the vortex core is stationary at this level and does not move in the axial direction. The axial resolution for the measurements of the EoV position was thus 3 cm.

Numerical Model

Computational grid and fluid conditions

Computational fluid dynamics (CFD) models were built to conform to the configuration of the swirl tubes used in the experiments. All geometrical and operational variables, including the shape of swirl vanes and vortex finder, were faithfully copied in the CFD models of the swirl tube. The three-dimensional (3-D) models were built in the commercial program Star Design, and discretization was performed using Star-CCM+ from CD-Adapco with a built-in cell trimmer.

After generation of the grids they were imported into Star-CD, which was used for the actual simulations. Figure 4 shows an overview of the grid geometry. To the left is the complete geometry showing all edges on the inside of the part of the cylindrical wall facing the viewer; in the center is the horizontal inlet into the tube section above the swirl vanes; and to the right is the entire upper section of the model where both the horizontal inlet and the swirl vanes are shown. The position and dimensions of the aforementioned vertical vanes for flow distribution have been duplicated from the experimental rig. The total number of cells were varied from 250,000 to 400,000, depending on the length of the swirl tube modelled. "Trimmed mesh," which combines the advantages of a near-regular mesh in the interior with a precisely fitting mesh at the walls, was used to build the CFD models, and the typical dimension of a cubical computational cell was 4 mm. But in the vanes region, that is, in the region with most complex geometry, the typical cell size was 2 mm.

As mentioned, pure air was chosen as the working fluid in the simulations. The temperature was taken as 293°K, and the air properties used were: density 1.205 kg/m^3, dynamic viscosity 1.81 $\times$ 10^{-5} Pa s and molecular mass 28.96 kg/kmol.

One problem with this detailed 3-D model was the huge amount of computational cells giving rise to a very long simulation times. For example, on a PC with Intel Core 2 CPU 2.4 GHz and 4 Gb of RAM, the simulation of 1 s of real time using

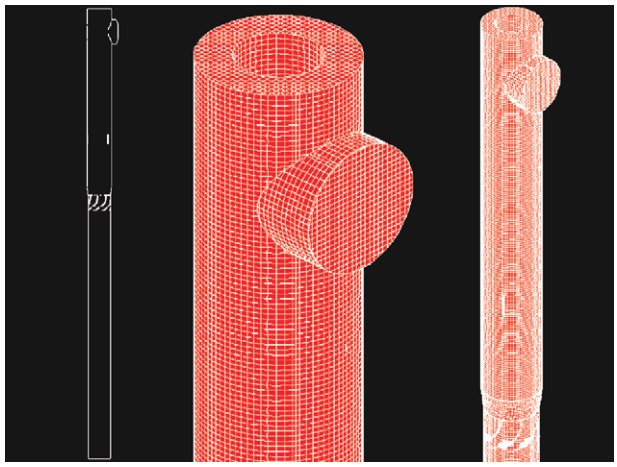

Figure 4. An overview of the CFD grid configuration.

Left: The complete geometry showing all edges on the inside of the part of the cylindrical wall facing the viewer. Center: Horizontal inlet into the tube section above the swirl vanes. Right: The entire upper section of the model with both the horizontal inlet and the swirl vanes. [Color figure can be viewed in the online issue, which is available at wileyonlinelibrary.com.]

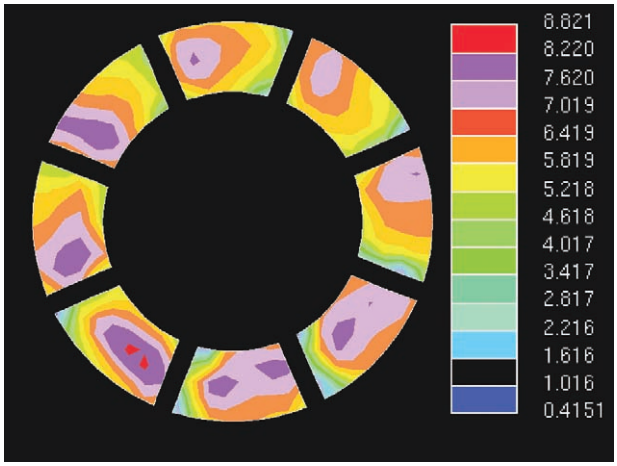

Figure 5. Velocity in cross-section of the top of the swirl vanes, m/s.

[Color figure can be viewed in the online issue, which is available at wileyonlinelibrary.com.]

a model consisting of 350,000 cells took about 8 h, and on a 24 core machine with 64Gb RAM the same simulation took about 3 h. The problem was that most of the cases required simulations of 1 min or more of real time. In spite of this, the cross-sectional flow at different axial positions in the tube between the flow distributors and the swirl vanes was investigated using this model. It was found that the velocity distribution of the air varied only slightly from one "compartment" between neighboring vanes to another, and at the top of the swirl vanes the velocity looked similar in all eight of the vane compartments (Figure 5). The inlet velocities were varied over the whole range of experimental data and this similarity was observed in all cases.

As the axial flow above the swirl vanes was found to be approximately similar, this gave us the opportunity to reduce the number of computational cells to almost half by cutting off the top part of the model right above the swirl vanes and assign an inflow boundary condition there. This reduced the time required for the simulations by a factor of at least four. The resulting simplified model is shown in Figure 6, the number of cells in this model varied between 35,000 and 180,000, depending on the length of swirl tube. In the region where the swirl vanes are located, the grid is refined to capture the details of the flow where the swirl is being generated.

Turbulence Model

Because of the nature of the phenomenon under study, the CFD simulation was needed to model the transient flow pattern. A crucial point for numerical simulations of confined turbulent flows is the correct choice of the turbulence model.

It is well-known that the standard k-ε model[11] cannot describe confined strongly swirling flow well, and it is to be expected that it cannot at all describe the phenomenon that we are interested in. However, to verify the actual results obtained, some preliminary simulations were carried out using the k-ε model. Deviations of the vortex core from the swirl tube axis were not obtained under any conditions and for any dimensions of separator with the k-ε model.

Many researchers assert that the Reynolds stress model (RSM) of the turbulence is suitable for this type of process. Simulations using RSM were also carried out. With this turbulence model the EoV phenomenon was, in fact, observed in the same velocity range as that used experimentally. The vortex core was observed bending to the wall and precessing around the wall. The position at which this occurred was lower at the higher flowrates. However, in detail the behavior of the EoV was not the same as in the experiments, for example, it would remain in a stable axial position on the wall at conditions under which it moved to the bottom of the tube experimentally.

Using these two turbulence models was, therefore, not sufficient to study the behavior of the EoV numerically.

The large eddy simulation (LES) turbulence model represents a major break-through in CFD,[12] reducing the empiricism involved in CFD and enabling modeling of complex flow phenomena. Hence, the LES model was chosen for this work.

LES involves a 3-D, time-dependent computation of the large-scale turbulent motions mainly responsible for turbulent mixing while those with scales smaller than the computational grid are parameterized. This parameterization of the subgrid turbulence can be in a rather simple form. In this study, the Smagorinsky model for μ_t was chosen as a simple, commonly used, and computationally inexpensive type of subgrid turbulence modeling for LES. The main assumption of this model was that of local equilibrium, that is, local rates of production and dissipation of subgrid turbulent stress were equal. The model had the following form[13,14]

$$\tau_{SGS,ij} - \frac{1}{3}\tau_{SGS,kk}\delta_{ij} = 2\rho C_{s2}\Delta^2\left\|\bar{s}_{ij}\right\|\bar{s}_{ij} = \mu_t\bar{s}_{ij} \qquad (1)$$

where $\left\|\bar{s}_{ij}\right\|$ represents the Frobenius norm of the filtered strain rate tensor $\bar{s}_{ij}$, Δ was taken as $V_{cell}^{1/3}$, ρ is the density of the gas, and μ_t is the dynamic viscosity. The parameter C_{s2} is taken to be the square of the classic Smagorinsky constant (0.165). We acknowledge that the classical value of 0.165 may be slightly high for the present system, which involves shear-induced turbulence in a confined flow.

For discretization the SIMPLE algorithm[15] with a three time-level temporal discretization was used. In this temporal discretization, the time derivative at time n in a given cell is estimated from the cell values at the two previous time steps

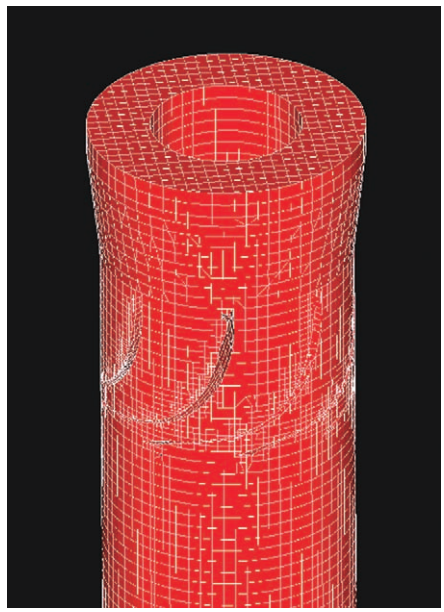

Figure 6. Numerical grid of the final model.

[Color figure can be viewed in the online issue, which is available at wileyonlinelibrary.com.]

$$\frac{d}{dt}\int_V \rho\phi dv \approx \frac{3(\rho\phi V)^n - 4(\rho\phi V)^{n-1} + (\rho\phi V)^{n-2}}{2\delta t} \quad (2)$$

This scheme has been found to be more stable than others for exactly the problem type we were interested in.

Boundary conditions

The boundary conditions were set in the following way. The fluid velocity was prescribed over the inlet boundary. Because of the experimental technique (suction by the pump in the physical experiments), this inlet boundary was set at the vortex finder, in other words, we had negative inlet in the model. Pressure boundary conditions were set at the inlet surface, where the pressures at the boundary cell faces were assumed to be known and equal to atmospheric pressure. The use of the negative inlet gives results in close agreement with experiment. This kind of boundary condition does, however, force a uniform velocity profile on that boundary and, therefore, does not fully represent flow behavior in the neighborhood of the outlet of cyclone. Earlier models, however, had the negative inlet placed higher in the vortex finder,[16] making this less of a problem, and the results in those models were consistent with those in the present model. A no-slip boundary condition was used on the wall boundary. The initial condition in the separator was taken as no-flow in all cases reported in this article.

The near-wall treatment was implemented as a two-step process. In the first step, the wall friction velocity, u_τ, is estimated by inverting a third-order Spalding law:

$$y^+ = u^+ + \frac{1}{E}\left(e^{ku^+} - 1 - ku^+ - \frac{(ku^+)^2}{2} - \frac{(ku^+)^3}{3!}\right) \quad (3)$$

where $u^+ = u/u_\tau$, E is an empirical coefficient, and k is the von Karman costant. In the second step, the relevant fluxes for momentum are computed on basis of an estimated u_τ.

In implementing the wall boundary conditions in the numerical scheme, it is important that the wall velocity is evaluated on the basis of the appropriate y^+ value, for example, when determining the velocity gradient at the wall.

Results and Discussion

We begin by discussing the results obtained in the experimental rig and then describe the numerical results.

In this article, the flow through the cyclone is given in m^3/h. The flow emanating from the vanes was assumed to be uniform. Therefore, the axial velocity from the vanes is $u_z = Q/(\pi(R^2 - R_v{}^2))$ with Q the volumetric flow in m^3/s, R the inner diameter of the tube, and R_v the inner diameter of the vanes. The tangential velocity emanating from the vanes is $u_\theta = u_z/\tan(\phi)$, where ϕ is the exit angle from the vanes relative to the horizontal. A Reynolds number for the cyclone can be defined based on the mean axial velocity in the swirl tube, $\bar{u}_z = Q/(\pi R^2)$

$$Re = \frac{\rho \bar{u}_z D}{\mu}$$

with $D = 2R$. A swirl number for the swirl tube can be defined as the ratio of the tangential to axial momentum flow from the vanes normalized by R

$$S \equiv \frac{G_\theta}{RG_z} = \frac{2\pi\int_{R_v}^{R}\rho u_z u_\theta r^2 dr}{R2\pi\int_{R_v}^{R}\rho u_z^2 r dr}$$

which, under the assumptions above, works out to

$$S = \frac{2\left(R^3 - R_v^3\right)\cot(\phi)}{3R\left(R^2 - R_v^2\right)}$$

S is thus fixed for the swirl tube and equals 1.53.

For a flow of, for example, 50 m^3/h $u_z = 4.04$ m/s, $u = 7.00$ m/s, $\bar{u}_z = 1.77$ m/s, and $Re = 11{,}800$. From an analogy with tangential-inlet cyclones u_θ can be taken as equivalent to the inlet velocity, which is also roughly equal to the tangential velocity at the wall of the swirl tube in the separation space in normal (not too long) swirl tube designs.

Experimental results

The results obtained in the different lengths of the swirl tube are discussed separately. In what follows the "length" of the swirl tube is defined as the distance from the bottom of the swirl vanes to the bottom of the separator, and "the distance from the swirl vane" means the distance from the bottom of the swirl vanes. The behavior of the vortex is described in some detail here, it is a flow system with a complex behavior.

35-cm Tube Length. Initially a relatively short swirl tube of 35 cm length was studied. Throughout the range of flowrates from 20 to 50 m^3/h, the vortex formed immediately (less than 1 s after starting the pump) and was observed to reach the bottom of the tube. This instant formation of a centralized vortex was, as mentioned, detected by motion of particles at the bottom of the separator. For flowrates lower than 20 m^3/h this motion was not observed, and pressure measurements did not detect the EoV on the walls of the swirl tube either. Consequently, it was reasonable to assume that for the range of flowrate lower than 20 m^3/h the gas flow did not form a vortex in the tube at all, and just flowed directly from the inlet (swirl vanes) to the gas exit (vortex finder). The threshold below which no vortex was formed was the same for all lengths of the swirl tube and will not be discussed further below. This threshold corresponded to a tangential velocity in the gas emanating from the vanes of 2.80 m/s, and it was consistent with practise that a vortex should not establish in tangential-inlet cyclones below approximately this inlet velocity.

45-cm Tube Length. For the 45-cm long swirl tube, the vortex also immediately formed on the bottom of the tube for flowrates in the range from 20 to 40 m^3/h. If the flow rate was higher, however (the range tested was from 40 to 50 m^3/h), the vortex would establish itself with the end attached to the separator wall, and then quikly move down to the bottom, taking 1.5–4 s to do so depending of the flowrate. The vortex always centralized in the end and its position on the wall was never stable during any period of time.

55- to 85-cm Tube Lengths. Experiments with a 55-cm long swirl tube started with flowrate of 25 m^3/h. During the first minute, there was no motion of the particles at the bottom indicating that the vortex did not reach the bottom of the swirl tube. After a minute, the pressure measurements detected the EoV at an axial position of 31 cm from the bottom of the swirl vanes. Examples of the pressure measurements will be shown below. It is interesting to mention that during increasing of the flowrate gradually with 3–5 m^3/h increments up to 50 m^3/h, the EoV stayed at this position and did not come down to the

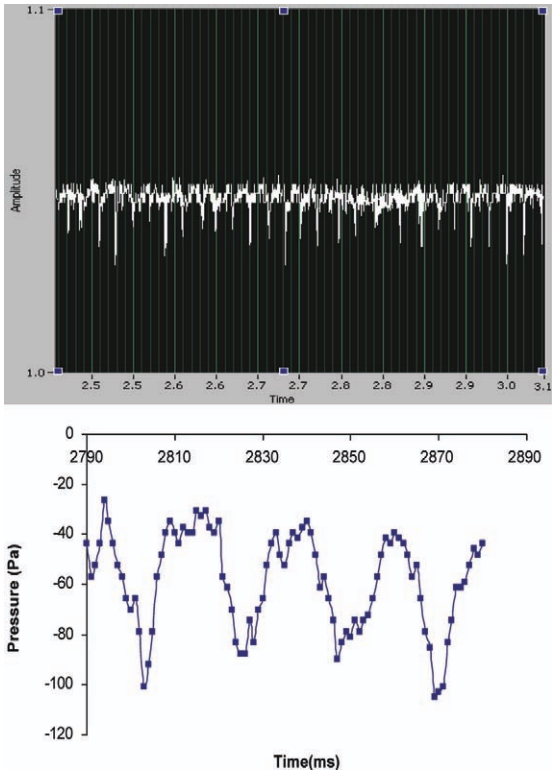

Figure 7. Pressure measurements at a flowrate of 75 m^3/h at 31 cm below the vanes.

Top: A time-series of the signals from a pressure tapping in volts. Bottom: Processed and converted to pressure signals in Pa. [Color figure can be viewed in the online issue, which is available at wileyonlinelibrary.com.]

bottom of the swirl tube, the pressure measurements showing the precessional motion of the vortex core. When increasing the flowrate to 51 m^3/h, the vortex core started its verical motion to the bottom and centralized 10 s thereafter. In addition to the described experiments where the flowrate was gradually increased from 25 m^3/h, experiments were performed wherein in flowrate from the start-up was in the interval from 40 to 50 m^3/h. For flowrates lower than 46 m^3/h, the same behavior of the vortex core as described at the beginning of this subsection was observed, that is, the EoV was initially observed on the wall, and the vortex core could be brought to the bottom by increasing the flowrate to above 51 m^3/h. However, when the startup flowrate was set to 47 and 48 m^3/h, the vortex, after initially appearing on the wall, centralized without increasing the flowrate, and this took 30 and 20 s for the two flowrates, respectively.

The same behavior of the vortex was observed for the 65, 75, and 85 cm lengths of the swirl tube. Also in these lengths, the EoV remained at the level of 31 cm under the swirl vanes. The only difference was detected in the flowrates required to centralize the vortex. When gradually increasing the flow as described above, the flowrates required for centralization of the vortex were 54, 62, and 73 m^3/h for the three tube lengths, respectively. When starting up at higher flowrates, as also described above, centralization of the vortex was observed at flowrates of 51, 58, and 70 m^3/h for the three respective lengths.

95-cm Tube Length. Experiments with 95-cm long swirl tube were also started at 25 m^3/h and the EoV was detected at 31 cm below the vanes, as for the previously discussed tube lengths. Increasing the flowrate beyond 80 m^3/h the EoV moved down to 14 cm above the bottom of the tube, remaining there. At 115 m^3/h, the vortex finally centralized. In this case, experiments with higher startup flowrates did not result in different threshold velocities compared with those found by gradually increasing the flow: at the flowrates less than 115 m^3/h the EoV remains at 14 cm from bottom, and at higher flowrates the vortex centralized.

Stability of the Centralized Vortex. After vortex centralization, the flowrate was always decreased to detect at which flowrate it would decentralize to form an EoV. For all the cases discussed here, the vortex, once centralized, in fact remained centralized for all flowrates as long as the decrease in flowrate was made gradually. Only strong disturbances like a very large and sudden drop in the flowrate to rates lower than 25 m^3/h could occasionally break it. So, for the flowrates down to 25 m^3/h, the position of the vortex core on the bottom of separator was stable and did not depend on the flowrate for all lengths of the swirl tube. There was thus a very strong hysteresis effect in the phenomenon of the EoV.

High-Speed Pressure Measurements. As mentioned, high-speed pressure measurements were performed using the pressure tappings positioned through the entire length of the separator. The pressure tapping measurements were performed if the position of the vortex core was not detected on the bottom of separator. In addition to detecting the EoV, another objective of these measurements was to estimate the frequency of rotation of the vortex core on tube wall. Figure 7 shows pressure measurements at the position of the EoV at 75 m^3/h in a 95 cm long swirl tube at 31 cm below the vanes. The frequency was estimated by counting cycles in a longer time-series (Figure 7; top) and found to be 49 s^{-1} for this case.

CFD results

Using the LES turbulence model it was possible to simulate the EoV phenomenon so that the vortex core was observed to bend from the axis of the cyclone and attach to the wall, around which it would precess in exactly the same way as it was observed experimentally during this and earlier projects.

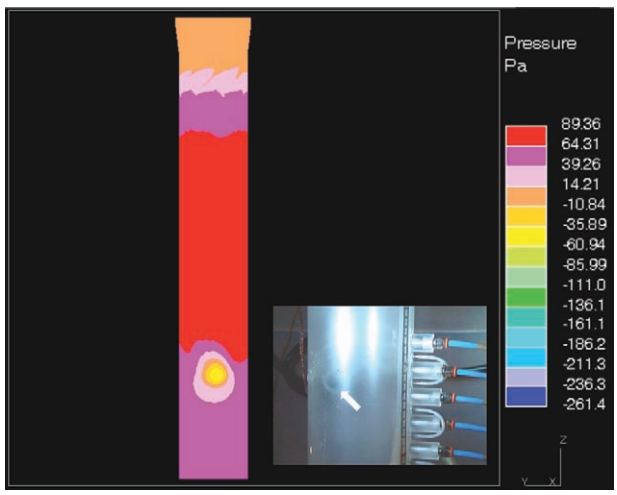

Figure 8. The vortex core on the wall of a swirl tube from CFD simulations shown as a profile plot for the pressure on the wall and from experiment.[3]

[Color figure can be viewed in the online issue, which is available at wileyonlinelibrary.com.]

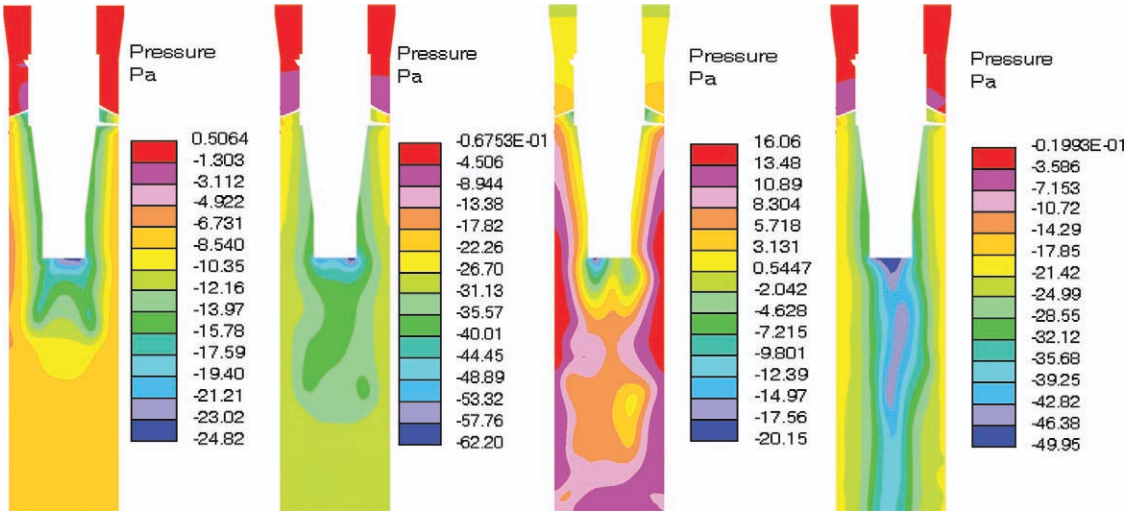

Figure 9. Contour plots at successive points in time of the static pressure in a 35 cm long swirl tube.

From left to right: 0.2, 0.4, 0.6 and 0.8 s. The flowrate is 50 m^3/h. [Color figure can be viewed in the online issue, which is available at wileyonlinelibrary.com.]

As discussed below, the global behavior of the phenomenon in the CFD simulations was very similar to the behavior in the experimental rig. Figure 8 shows the vortex core in the numerical simulations as a profile plot of the pressure on the wall together with a photo taken on the wall of a swirl tube with the help of a strobe light in earlier experiments.[3]

Below, the results for the different tube lengths are discussed separately.

35-cm Tube Length. Matching the experimental results, the CFD simulations in the 35 cm tube showed that between the flowrates of 25 and 50 m^3/h the vortex formed immediately and was centralized when formed, more precisely the vortex formed within 0.4 to 0.8 s, depending on the flowrate. Figure 9 shows one example of the process of centralization of the vortex. As mentioned, the initial condition for all the simulations is one of now flow.

45-cm Tube Length. Also for this tube length the CFD simulations matched the experimentally observed behavior. At flowrates under 40 m^3/h, the vortex formed almost immediately and was centralized when formed, taking 0.5–1 s to form depending on the flowrate. However, when the flowrate was increased beyond this threshold, the vortex core was bent to the the wall in an EoV on formation of the vortex and the EoV took several seconds to move to the bottom of the tube for the vortex to centralize. The exact time required for final centralization depended on the flowrate. Figure 10 shows an example of how the centralization took place during time.

55- to 75-cm Tube Lengths. For CFD models of swirl tubes with lengths ranging from 55 to 75 cm approximately, the same behavior as for the 45 cm length was observed. For flowrates below 30 m^3/h, the vortex was formed centralized. For flowrates higher than 30 m^3/h, the vortex would bend to the wall on formation and then move down to centralize, and the time taken in doing so depending on the flowrate. The vortex would always centralize in the end but, for example, for a tube of 75 cm length and with a flowrate of 37 m^3/h the process of centralization took more than 1 min of real time.

85- to 95-cm Tube Lengths. For these lengths it was, like for the shorter lengths, observed that the vortex would centralize on formation without first bending to the wall in simulations with flowrates lower than 30 m^3/h. In simulations with a flowrate of 30 m^3/h and a tube length of 85 cm, the vortex would bend to the wall, move down, but remain at some level on the wall, this case then results in a stable flowpattern with the EoV present. However, in the simulation with 35 m^3/h for the same tube length, the vortex, after initially exhibiting an EoV, centralized after 50 s. In fact, in the narrow range of flowrates of 30–35 m^3/h (± 1 m^3/h) the EoV is present in a stable position. Further simulations showed that the exact position of the EoV depends on the flowrate and was found to be in the range of 30–20 cm from the bottom. Similar results were obtained for the tube length of 95 cm, but the range wherein the EoV took up a stable position was estimated to be slightly wider: 30–40 m^3/h, and the stable positions were in the range of 40–20 cm from the bottom of separator, closer to the bottom for the higher flowrate. Figure 11 shows simulations in the 95 cm tube wherein the position of the EoV is stable.

Stability of the Centralized Vortex. As in the experimental program whenever the vortex centralized and after centralization the flow in the CFD model was decreased gradually to 20 m^3/h to see if the vortex would remain centralized. The behavior was the same as in the experimental results. After the vortex had centralized it remained centralized in all cases, the flow phenomenon of the EoV thus exhibiting a strong hysteresis effect also in the CFD simulations.

Pressure Measurements. We also investigated the temporal history of the static pressure in a computational cell, the axial position of which was at the EoV location. An example is represented in Figure 12. In the CFD simulations, the EoV did not remain on the wall at a flowrate of 75 m^3/h. However, to compare with the experimental data given in Figure 7, a time-series of the pressure at the wall 31 cm below the vanes was recorded at the moment the EoV passed this position on its way to the bottom of the tube. The frequency for this case was estimated on basis of a long time series to be 48 s^{-1}.

Grid Independence. Test for grid indepence was carried out in the following way. A simulation in the normal grid consisting of 92,991 cells was repeated with a much finer grid consisting of 296,520 cells. The pressure fields from the two simulations corresponding to the exact same point in time were then rendered and compared.

Figure 13 shows the two pressure fields. Obviously in LES, the pressure and the velocity fluctuate randomly around

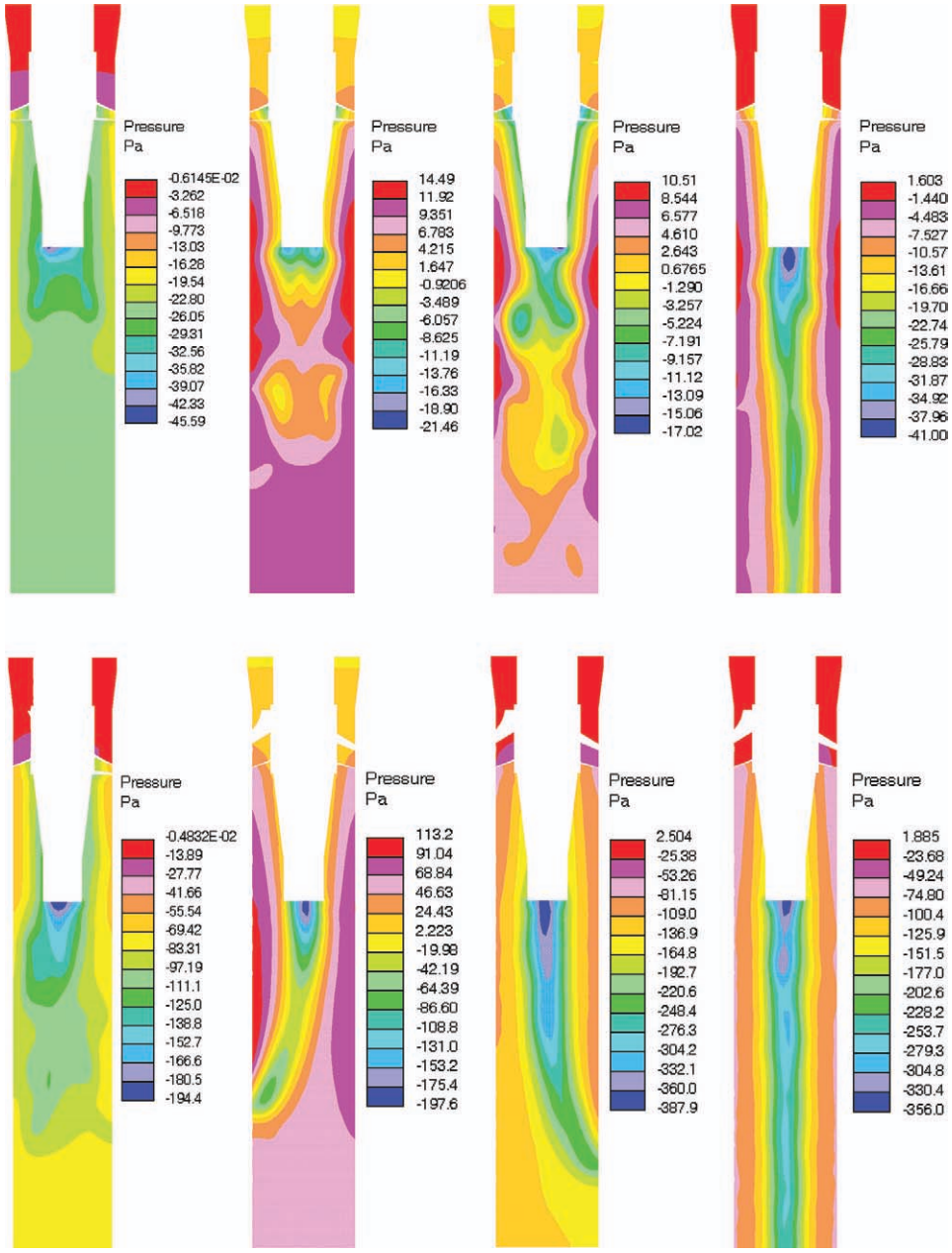

Figure 10. Contour plots at successive points in time of the static pressure in a 45 cm long swirl tube.

Top four images from left to right: 0.2, 0.4, 0.6 and 0.8 s with a flowrate of 35 m^3/h. Bottom four images from left to right: 0.2, 0.4, 1 and 2 s with a flowrate of 50 m^3/h. [Color figure can be viewed in the online issue, which is available at wileyonlinelibrary.com.]

their mean values, and it is only possible to compare the mean flow field by inspecting the overall flowpattern.

It can be seen from the figure that the two simulations have resulted in the same angular and axial positions, to within a couple of centimeters, for the precessing vortex core demonstrating that the numerical results shown above are grid independent. A study of the color legends of both figures show that the absolute pressures are the same within a few percent almost everywhere in the two flow fields.

Further remarks

Comparison of the experimental and CFD results shows excellent agreement for tube lengths of 35 and 45 cm.

For the longer lengths, the agreement was also very good. There were, however, some differences between experiment and CFD for these lengths. We think that these differences may, in part, be attributed to the joints in the experimental tubes. The tube of 55 cm was made from two sections, 30 and 20 cm long, and that of 95 cm from three sections of 35, 50, and 10 cm. The stable EoV positions at 31 cm below the vanes and 14 cm from the bottom seen experimentally but not in the simulations may be due to the EoV being "caught" above the joints, requiring a considerable increase in the flow to force it to pass these positions. This may also be the reason for the difference in experimental and CFD EoV positions in the 85 cm tube. This in spite of considerable efforts to make the joints as smooth as possible. It is, in itself, an interesting result for cyclone designers that the phenomenon is so dependent on small disturbances on the wall. Further work will be done to investigate this.

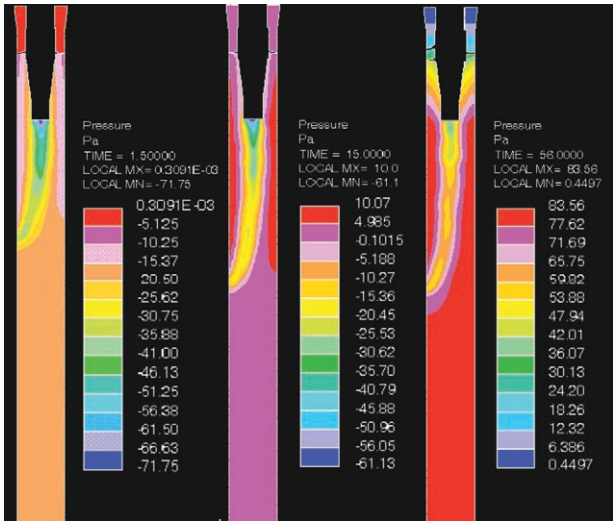

Figure 11. Simulations wherein the EoV remains at a stable position on the tube wall in the 95-cm swirl tube.

[Color figure can be viewed in the online issue, which is available at wileyonlinelibrary.com.]

Nevertheless, overall, the agreement was surprisingly good.

Also the pressure measurements show good agreement, the differences between experiment and CFD being only about 5%. One could not expect better agreement in light of the fact that the pressure tapping may not be aligned precisely with the center of the EoV in the experimental rig, even though the pressure tappings were very closely spaced.

Conclusions and Further Comments

Experimental and numerical investigation of one type of reverse-flow centrifugal separators, namely cylindrical swirl tubes, have been carried out.

It has been shown that the instability in the vortex flow leading to the formation of the end of the vortex can be simulated numerically using the LES turbulence model and that the behavior of this phenomenon is—even in detail and to some extent qualitatively—consistent with what is seen experimentally. Depending on the length of the tube three possible scenarios were observed.

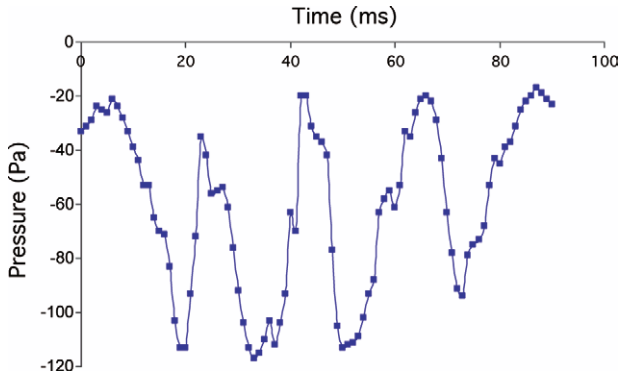

Figure 12. Time-series of pressure at a point on the wall at the position of the EoV. The flowrate is 75 m^3/h.

[Color figure can be viewed in the online issue, which is available at wileyonlinelibrary.com.]

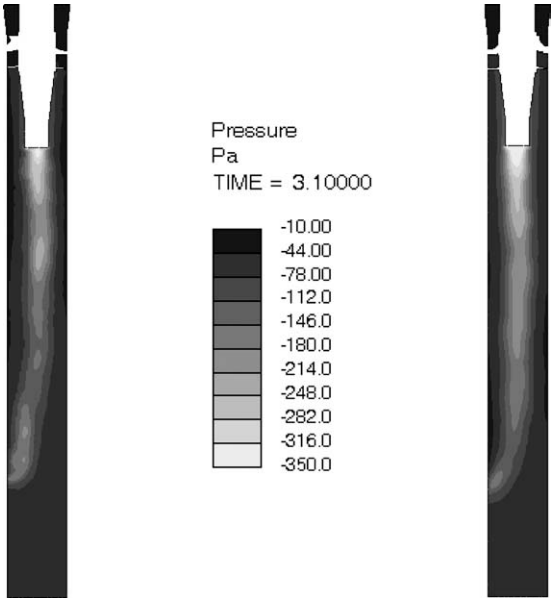

Figure 13. Comparison of the pressure fields at a given instant in time with different computational grids.

Left: Simulation in the refined grid consisting of 296,520 cells. Right: Simulation in the normal grid consisting of 92,991 cells. Flowrate: 70 m^3/h.

1. The vortex is stable and centralized on formation.
2. The vortex core initially bends to the wall, rotates on it, and descends, finally reaching the bottom after some period of time; this is probably related to start-up effects as the flow in the tube is established.
3. The vortex core bends to the wall of the separator, rotates on it, and slowly descends but stops at some level from the bottom, where it remains forming a flowpattern with a stable EoV.

Very good agreement between experimental and numerical study has been observed.

We acknowledge that the tube used here is small compared to most industrial scales. However, problems related to the EoV are no less relevant on larger scales. Some of the authors have worked with projects related "third stage separators" (TSS), and EoV problems are very relevant there also. Also unmistakable evidence of the EoV in cylinder-on-cone cyclones 4 m in diameter in the cement industry is present. Scaling numerical simulations based on Reynolds number similarity is an easy and, as this study indicates, relevant way of studying this.

The swirl tubes in this study operated at Reynolds numbers, based on the mean axial velocity, of 5000–27,000, while a typical TSS operating at 14 m/s axial velocity on hot flue gases[8] operates at a Reynolds number of 97,000.

Two priorities for further research will be to carry out a stability analysis for the centralized flow to determine the factors influencing the onset of the EoV phenomenon and studying the effects of the presence of the EoV on the flow of particles in the separator.

Acknowledgments

The Norwegian Research Council is gratefully acknowledged for funding this work through the FRINAT programme.

Literature Cited

1. Hoffmann AC, Stein LE. *Gas Cyclones and Swirl Tubes, Principles, Design and Operation*, 2nd ed. Berlin, Heidelberg, New York: Springer, 2007.
2. Zhongli J, Xiaolin W, Mingxian S. Experimental research on the natural turning length in the cyclone. Proceedings of Filtech Europa 91, vol. 2, 1991:583–589.
3. Peng W, Hoffmann AC, Dries HWA, Regelink MA, Stein LE. Experimental study of the vortex end in centrifugal separators: the nature of the vortex end. *Chem Eng Sci*. 2005;60:6919–6928.
4. Hoffmann AC, Dejonge R, Arends H, Hanrats C. Evidence of the natural vortex length and its effect on the separation efficiency of gas cyclones. *Filtr Sep*. 1995;32:799–804.
5. Alexander R. Fundamentals of cyclone design and operation. Proceedings Aus. I.M.M., vol: 152–153, 1949:203–228.
6. Bryant HS, Silverman RW, Zenz FA. How dust in gas affects cyclone pressure-drop. *Hydrocarbon Process*. 1983;62:87–90.
7. Qian FP, Zhang MY. Study of the natural vortex length of a cyclone with response surface methodology. *Comput Chem Eng*. 2005;29: 2155–2162.
8. Peng WM, Hoffmann AC, Dries H. Separation characteristics of swirl-tube dust separators. *AIChE J*. 2004;50:87–96.
9. Barth W. Berechnung und auslegung von zyklonabscheidern auf grund neuerer unterscuhungen. *Brennstoff-Wärme-Kraft in German*. 1956;1:1–9.
10. Raoufi A, Shams M, Farzaneh M, Ebrahimi R. Numerical simulation and optimization of fluid flow in cyclone vortex finder. *Chem Eng Process*. 2008;47:128–137.
11. Balakin BV, Hoffmann AC, Kosinski P, Hoiland S. Turbulent flow of hydrates in a pipeline of complex configuration. *Chem Eng Sci*. 2010;65:5007–5017.
12. Derksen JJ, van den Akker HEA. Simulation of vortex core precession in a reverse-flow cyclone. *AIChE J*. 2000;46:1317–1331.
13. Ferziger JH, Peri M. *Computational Methods for Fluid Dynamics. The Basics with Applications*, 3rd ed. Heidelberg: Springer, 2003.
14. Piomelli U. Large-eddy simulation: achievements and challenges. *Progr Aerospace Sci*. 1999;35:335–362.
15. Patankar SV. *Numerical Heat Transfer and Fluid Flow*. Washington: Hemisphere Publ. Corp., 1980.
16. Pisarev GI, Hoffmann AC, Peng W, Dijkstra HA. Large eddy simulation of the vortex end in reverse-flow centrifugal separators. *Appli Math Comput*. 2011;217:5016–5022.

Manuscript received Dec. 6, 2010, and revision received May 3, 2011.